4. DATA RESOURCE

Wind pressures on the surfaces of the rigid model of a tall building were measured for a long time in the boundary layer wind tunnel at Dalian University of Technology, China. The working section of the wind tunnel laboratory is 3 m in width, 2.5 m in height, and 18 m in length. Spires and roughness cube elements were used to generate the desired boundary layer wind profile. A boundary layer corresponding to the urban terrain (Category C) in Chinese code GB50009-2012 (National Standard of the People's Republic of China, 2012) was simulated.

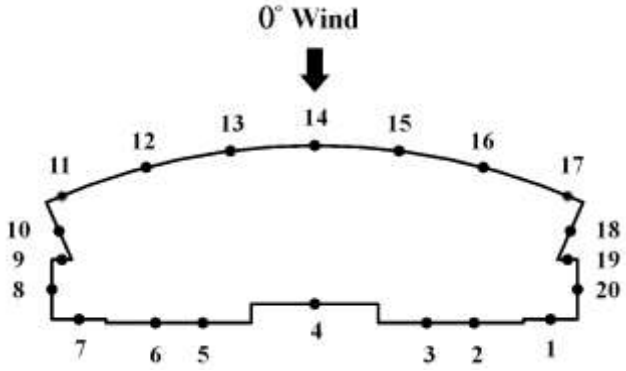

Fig. 1 Arrangement of pressure taps and wind directions

Fig. 2 A picture of the wind tunnel test

The tests were conducted on a 54 cm high rigid model with a length scale of 1: 200. The velocity scale was set as 1: 4, and the corresponding time scale was 1: 50. The plane layout of Taps 1-20 and a picture of the test are respectively shown in Fig. 1 and Fig. 2. The sixty taps on the three layers, i.e., at the height of 23, 35, and 46cm, were numbered as 1-20, 21-40, and 41-60, respectively. At a sampling frequency of 312.5 Hz, a long time history of 20 min was recorded in 0° wind direction as shown in Fig. 1. Correspondingly, the time duration for full-scale measurement was 1000 min, i.e., 100 repeats of 10-min standard time intervals.

5. COMPARISON of FITTING GOODNESS for NON-GAUSSIAN DISTRIBUTION

In this section, the Bayesian-based HPM and the MM-based HPM will be applied to model the wind pressure records, and their fitting performance will be compared. Two taps, i.e., No. 1 and No. 7 are taken as the computational examples. The long-duration time histories are divided into 100 segments with 10-min standard time intervals. The skewness and kurtosis of the total 200 segments of two taps are dotted in Fig. 3.

Due to the randomness of aerodynamic effect and the incomplete ergodicity of collected data, the statistics of short segments exhibit random properties as shown in Fig. 3, which violates the assumption of constants. However, for the MM, e.g., in Eq. (4),

the γ_3 and γ_4 are considered as the constants which are equal to the skewness and kurtosis of the samples. Substitute these γ_3 and γ_4 into Eq. (4), the calculation results of h_3 and h_4 are dotted in Fig. 4. It is obvious that the shape parameters of HPM also show the random characteristics.

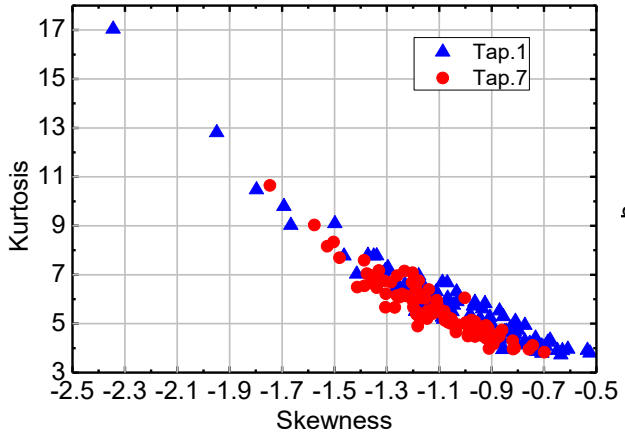

Fig. 3 Skewness and kurtosis of wind pressures

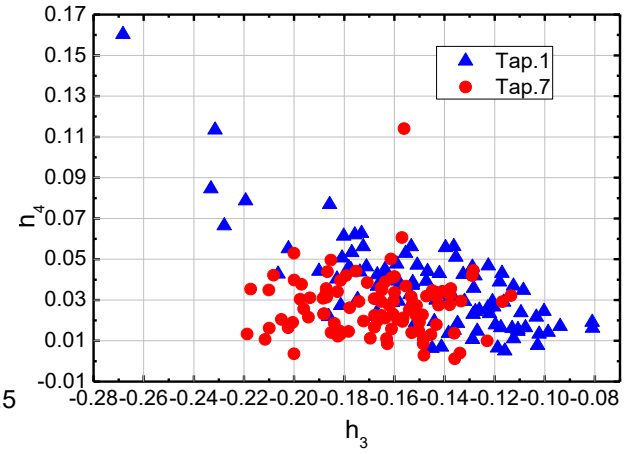

Fig. 4 h_3 and h_4 for two taps

The variance of the statistical moments becomes lower when the length of the segments increases. Only if the length of segments were assigned long enough, the statistical moments could be approximated as constants. Nevertheless, the wind tunnel tests and field measurements are always kept for a quite short time, e.g., less than 1min for wind tunnel tests, which probably leads to the skewness and kurtosis of the sample deviate farther away from their expected values. It also affect the estimation accuracy of the shape parameters h_3 and h_4. In Bayesian method, h_3 and h_4 are considered as variables, and the probable errors caused by the randomness of sampled data can be theoretically reduced. The following discussion is conducted on the basis of the assumption that only the first 1min, i.e., the five segments are in hand. The standardized time histories of the first five segments at the two taps are plotted in Fig. 5, and their skewness and kurtosis are also listed.

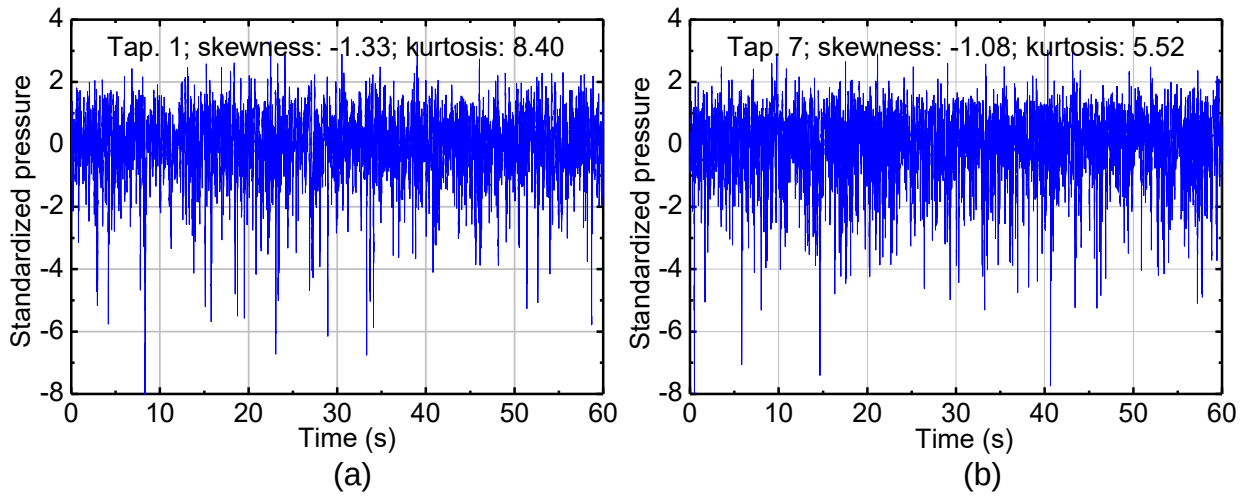

Fig. 5 Time histories of wind pressure at two taps: (a) Tap 1; (b) Tap 7

Two sets of shape parameters in HPM are respectively calculated by Eq. (4) and the proposed Bayesian method. The corresponding PDF curves are plotted in Fig. 6. The real target of the utilization of HPM is to predict the long-term probabilistic characteristics by using the short-term sampled data in hand. Therefore, the histograms of the total 100 segments are also shown in Fig. 6 as the benchmark reference for assessing the fitting goodness. The skewness and kurtosis of the entire sampled data is -1.08 and 6.16 for Tap 1, -1.14 and 5.80 for Tap 7, respectively. The third- and fourth- moments of the short-term data for Tap 7 are very close to the statistics of the entire data. However, the corresponding pairs deviates far from each other for Tap 1. Therefore, the MM-based HPM fits the histogram of Tap. 7 quite well in the bulk, due to the statistics of short-term data for Tap. 7 in hand is close to the long-term data coincidentally. But it lose accuracy for Tap. 1, because of the big difference between the statistics of short-term data in hand and the long-term data. By comparison, the Bayesian-based HPM offered both taps outstanding fit in the mean region. For further exploring the fitting performance of two methods for the tails area, the semi-log scales comparisons of PDF are shown in Fig. 7.

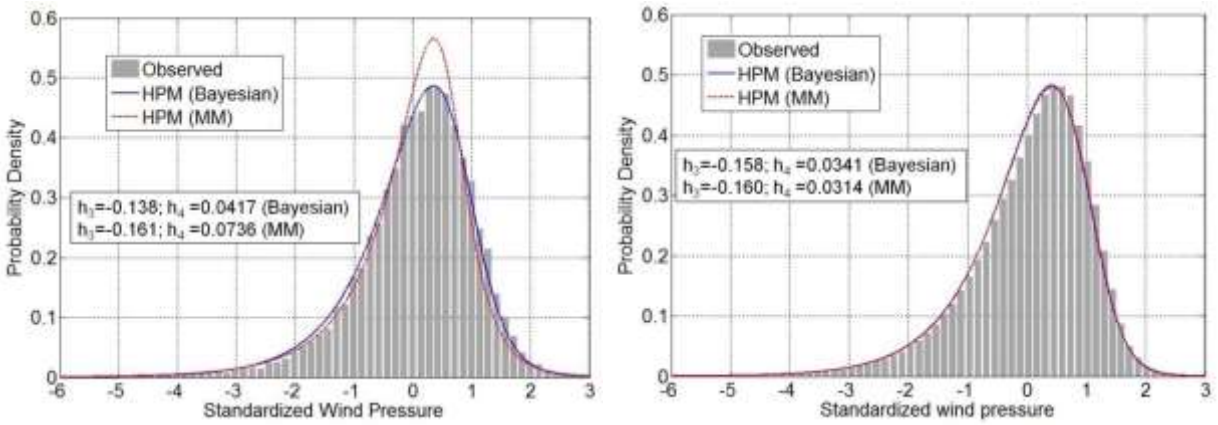

(a) (b)

Fig. 6 Comparisons of fitted PDFs (a) Tap 1; (b) Tap 7

The comparative results in tail areas are similar to those in the mean region. The Bayesian-based HPM did much better than the MM-based HPM for Tap 1 on both long-tail and short-tail side.

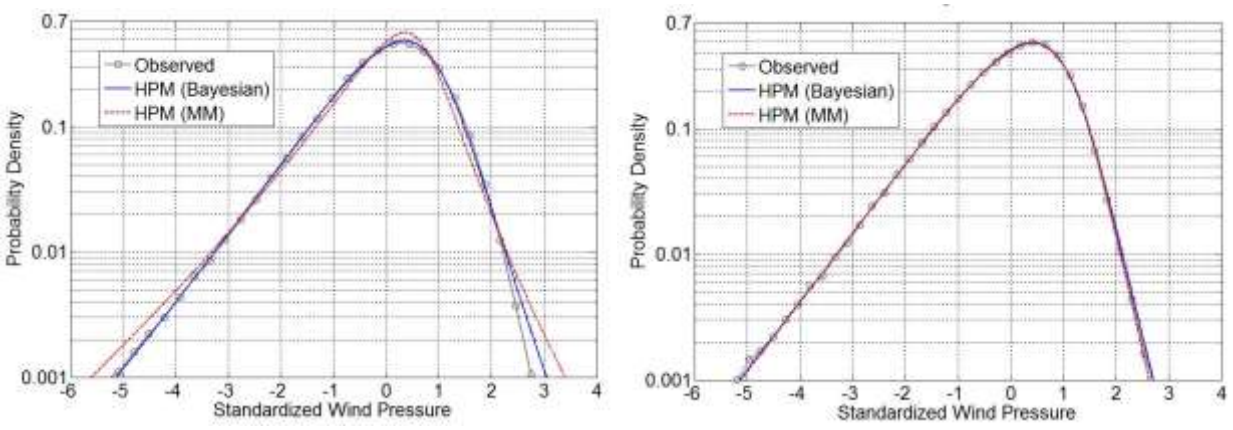

Fig. 7 Comparisons of fitted PDFs in semi-log scale (a) Tap. 1; (b) Tap. 7

6. Estimation of Wind Pressure Extrema

After the parent non-Gaussian distribution is fitted by the HPM, the CDF of the non-Gaussian extrema can be estimated (Kwon and Kareem 2011). Due to the extrema on the long-tail side of the non-Gaussian distribution are relatively larger than those on the short-tail side, the extrema on long-tail side is usually of more interest for structure design. Accordingly, the estimated CDFs of extrema on the long-tail side from two methods are plotted in Fig. 8. The empirical CDF of the minimum values from 100 segments are also plotted in Fig. 8 as the standard value for comparison. Meanwhile, the lower and the upper confidence bounds (LCB and UCB) at the confidence level of 95% are also calculated and marked. For Tap. 7, both methods matches the empirical CDF well. The derived extrema CDFs is located between the LCB and the UCB. The good performance is beneficial from the high-level fitting of the parent distribution as shown in Fig. 7b. However, there is an obvious gap between the matching goodness of two methods for Tap 1. The estimation from MM-based HPM lost its accuracy, but the estimation from Bayesian-based HPM still matches the empirical CDF outstandingly, by which the accuracy of the Bayesian-based method is convincingly demonstrated.

A further discussion is conducted by integrating the Fig. 7 and 8. The accurate estimation of the probabilistic properties of the extrema requires accurate fitting of the parent distribution. However, if the sampled data in hand is not long enough, their statistics cannot be regarded as constants. Once they are considered as constants, for instance in the method of moment and the method of maximum likelihood, the fitting accuracy of parent distribution cannot be guaranteed.

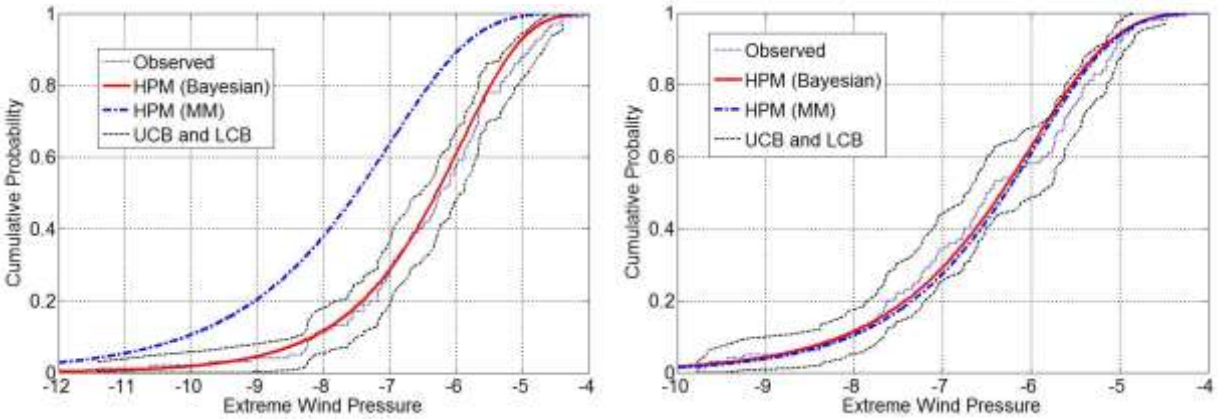

Fig. 8 Comparisons of extrema CDF on the long-tail side: (a) Tap 1; (b) Tap 7

7. Concluding Remarks

In this study, a Bayesian-based method is proposed to calculate the shape parameters of the Hermite polynomial model (HPM). Based on the long-duration wind pressure records on the surfaces of a high-rise building model in wind tunnel tests, the parent non-Gaussian distributions at two Taps were fitted by the Bayesian method and the conventional method (method of moment). The fitting goodness of the two methods is comprehensively compared and analyzed. Compared with conventional method, the Bayesian-based method has a better fitting performance of non-Gaussian distribution in both bulk and tail regions. The estimation accuracy of the extrema CDF by the new method is also fully verified by comparing with the conventional method and the directly observed results.

Acknowledgement
The research is jointly supported by the National Program on Key Basic Research Project (973 Program, 2015CB057705) and National Science Foundation of China (51478087).

REFERENCES

Ding, J., and Chen, X. Z. (2015). “Moment-Based translation model for hardening non-Gaussian response processes.” J. Eng. Mech., ASCE, 06015006.

Huang, M. F., Lou, W., Pan, X., Chan, C. M., and Li, Q. S. (2014). “Hermite Extreme Value Estimation of Non-Gaussian Wind Load Process on a Long-Span Roof Structure.” Journal of Structural Engineering, ASCE, 140(9): 04014061.

GB 50009-2012. (2012). Load code for the design of building structures, Architecture Industrial Press of China, Beijing (in Chinese).

Grigoriu, M. (1984). “Crossings of non-Gaussian translation processes.” J. Eng. Mech., ASCE, 110(4): 610-620.

Gurley, K. R., Tognarelli, M. A., and Kareem, A. (1997). “Analysis and simulation tools for wind engineering.” Probabilistic Engineering Mechanics, 12(1): 9-31.

Hastings, W. K. (1970). “Monte Carlo sampling methods using Markov chains and their applications.” Biometrika, 57(1):97-109.

Holmes, J. D., and Cochran, L. S. (2003). “Probability distributions of extreme pressure coefficients.” J. Wind Eng. Ind. Aerodyn., 91(7): 893-901.

Huang, M. F., Lou, W., Pan, X., Chan, C. M., and Li, Q. S. (2014). “Hermite Extreme Value Estimation of Non-Gaussian Wind Load Process on a Long-Span Roof Structure.” J. Struct. Eng., ASCE, 140(9): 04014061.

Ishikawa, T. (2004). “A study on wind load estimation method considering dynamic effect for overhead transmission lines.” PhD thesis, Waseda University.

Kasperski, M. (2003). “Specification of the design wind load based on wind tunnel experiments.” Journal of Wind Engineering and Industrial Aerodynamics, 91(4): 527-541.

Kwon, D. K., and Kareem, A. (2011). “Peak factors for non-Gaussian load effects revisited.” J. Struct. Eng., ASCE, 137(12): 1611-1619.

Li, Q. S., and Hu, S. Y. (2015) “Monitoring of wind effects on an instrumented low-rise building during severe tropical storm.” Wind and Structures, 20(3):469-488.

Masters, F., and Gurley, K. R. (2003). “Non-Gaussian simulation: Cumulative distribution function map-based spectral correction.” J. Eng. Mech., ASCE, 129(12):1418-1428.

Metropolis, N., Rosenbluth, A. W., Rosenbluth, M. N., Teller, A., and Teller, A. H. (1953). “Equation of state calculations by fast computing machines.” J. Chem. Phys., 21(6), 1087–1092.

Tognarelli, M. A., Zhao, J., and Kareem, A. (1997). “Equivalent statistical cubicization for system and forcing nonlinearities.” J. Eng. Mech., 123(8), 890–893.

Winterstein, S. R. (1985). “Non-normal responses and fatigue damage.” J. Eng. Mech., 111(10), 1291–1295.

Winterstein, S. R. (1988). “Nonlinear Vibration Models for Extremes and Fatigue.” J. Eng. Mech., ASCE, 114(10): 1772-1790.

Winterstein, S. R., Ude, T. C., and Kleiven, G. (1994). “Springing and slow-drift responses: predicted extremes and fatigue vs. simulation.” Proceedings, Behaviour of Offshore Structures at Sea -- BOSS-94, 3:1-15.

Winterstein, S. R., and Kashef, T. (2000). “Moment-based load and response models with wind engineering applications.” J. Sol. Energy Eng., 122, 122–128.

Winterstein, S. R., and Mackenzie, C. A. (2011) "Extremes of Nonlinear Vibration: Models Based on Moments, L-Moments, and Maximum Entropy." Journal of Offshore Mechanics and Arctic Engineering, 135(2):185-195.

Yang, L. P., Gurley, K. R., and Prevatt, D. O. (2013). “Probabilistic modeling of wind pressure on low-rise buildings.” J. Wind Eng. Ind. Aerodyn., 114: 18-26.

Yang, Q. S., and Tian, Y. J. (2015). “A model of probability density function of non-Gaussian wind pressure with multiple samples.” Journal of Wind Engineering and Industrial Aerodynamics, 140:67-78.